gut microbes



Taylor & Francis
Taylor & Francis Group

Science and Technology of Advanced Materials

ISSN: 1468-6996 (Print) 1878-5514 (Online) Journal homepage: www.tandfonline.com/journals/tsta20

Reorientational dynamics of amino acids in aqueous solution probed by ultrafast optical kerr effect spectroscopy

Koichi Murakami, Tomohiro Nobeyama, Yuta Koda, Takahiro Sasamori, Kentaro Shiraki, Yohei Yamamoto & Soh Kushida

To cite this article: Koichi Murakami, Tomohiro Nobeyama, Yuta Koda, Takahiro Sasamori, Kentaro Shiraki, Yohei Yamamoto & Soh Kushida (21 Sep 2026): Reorientational dynamics of amino acids in aqueous solution probed by ultrafast optical kerr effect spectroscopy, Science and Technology of Advanced Materials, DOI: 10.1080/14686996.2026.2736324

To link to this article: https://doi.org/10.1080/14686996.2026.2736324

© 2026 The Author(s). Published by National Institute for Materials Science in partnership with Taylor & Francis Group.

View supplementary material

Accepted author version posted online: 21 Sep 2026.

Submit your article to this journal

Article views: 6

View related articles

View Crossmark data

Full Terms & Conditions of access and use can be found at
https://www.tandfonline.com/action/journalInformation?journalCode=tsta20

Check for updates

Publisher: Taylor & Francis & The Author(s). Published by National Institute for Materials Science in partnership with Taylor & Francis Group.

Journal: *Science and Technology of Advanced Materials*

DOI: 10.1080/14686996.2026.2736324

Reorientational dynamics of amino acids in aqueous solution probed by ultrafast optical Kerr effect spectroscopy

Koichi Murakami[a], Tomohiro Nobeyama[a,b], Yuta Koda[a], Takahiro Sasamori[a], Kentaro Shiraki[a], Yohei Yamamoto[a,c]*, and Soh Kushida[a]*

[a] *Institute of Pure and Applied Sciences, University of Tsukuba, Japan,* [b]*The Hakubi Center for Advanced Research, Kyoto University, Japan.* [c]*Tsukuba Research Center for Energy Materials Science (TREMS) and Hydrogen Boride Research Center, Tsukuba Institute for Advanced Research, University of Tsukuba*

*corresponding author:

Dr. Soh Kushida, Institute of Pure and Applied Sciences, University of Tsukuba, Tsukuba 305-8573, Japan

Prof. Yohei Yamamoto, Institute of Pure and Applied Sciences, Tsukuba Research Center for Energy Materials Science (TREMS) and Hydrogen Boride Research Center, Tsukuba Institute for Advanced Research, University of Tsukuba, Tsukuba 305-8573, Japan

orcid.org/0000-0002-4474-9529

Email: s-kushida@ims.tsukuba.ac.jp, yamamoto@ims.tsukuba.ac.jp

ACCEPTED MANUSCRIPT

Provide short biographical notes on all contributors here if the journal requires them.

ACCEPTED MANUSCRIPT

Reorientational Dynamics of Amino Acids in Aqueous Solution Probed by Ultrafast Optical Kerr Effect Spectroscopy

Reorientational relaxation of a solute in aqueous solution reflects the friction from its surroundings, yet observing this rotational motion solute by solute at the microscopic level is difficult. Ultrafast optical Kerr effect (OKE) spectroscopy can follow molecular reorientational relaxation in liquid phase, but it is not obvious whether the slow picosecond component arises from the rotation of the solute itself or from water slowed by the increased viscosity when it is applied to aqueous solution systems. Here, we use OKE spectroscopy to investigate the reorientational dynamics of three amino acids (alanine, proline, and lysine monohydrochloride) in aqueous solution in terms of concentration, temperature, and chirality. Using poly(vinyl alcohol) (PVA) as a control, we found that increasing the macroscopic viscosity by approximately eightfold did not alter the reorientational relaxation time of water. This result indicates that OKE provides information on the local rotational friction associated with the solute and highlights its unique role as a technique complementary to rheometry, which measures macroscopic viscosity. This study provides new insight into the local rotational environment experienced by solutes in aqueous amino acid solutions.

Keywords: amino acids; optical Kerr effect spectroscopy; reorientational dynamics

Introduction

Molecules in solution continually change their orientation through thermal motion. The rate of this reorientation reflects the friction between solutes and their surroundings at the local environment. This has long been discussed in the framework of Stokes–Einstein–Debye relation[1]. Observing the microscopic rotational dynamics of an individual solute in aqueous solution is, however, difficult. Ultrafast optical Kerr effect (OKE) spectroscopy is a time-resolved nonlinear optical method that measures the transient birefringence induced by an ultrashort pump pulse; the decay of the OKE signal reflects the reorientational relaxation of liquid-phase molecules on the femto- to picosecond timescale[2]. OKE spectroscopy has been applied to a wide range of liquid systems, including simple liquids, ionic liquids, and liquid crystals[1,3]. However, most conventional OKE studies have focused on neat liquids. Direct investigations of solute

ACCEPTED MANUSCRIPT

reorientational dynamics remain comparatively limited because the non-resonant OKE response contains contributions from all components, making it difficult to distinguish the solute response from the generally more abundant solvent background. When solute-specific dynamics have been targeted, resonant OKE has therefore often been employed, in which the excitation wavelength is tuned to an electronic transition of the solute to enhance its contribution[4]. Although this resonant enhancement provides much greater sensitivity to the solute dynamics, the range of application is generally restricted to chromophoric molecules, particularly molecular dyes possessing a distinct absorption band. Consequently, resonant OKE is not readily applicable to nonchromophoric solutes, such as many small aliphatic molecules and amino acids, that lack a suitable electronic absorption band in the visible region. By contrast, only a limited number of studies have employed non-resonant OKE to investigate the reorientational dynamics of solutes in aqueous solution[1–3,5–14].

Most aqueous OKE studies have rather focused on how dissolved species perturb the structure and dynamics of the surrounding water. For example, Meech and co-workers have used OKE spectroscopy to elucidate how solutes such as urea, ionenes, and acetate modify the hydrogen-bond structure and dynamics of water[6,7,14]. Righini and co-workers investigated the temperature dependence of the reorientational dynamics of aqueous urea and showed that its relaxation behavior was consistent with the Debye–Stokes–Einstein framework[7]. Nevertheless, in a non-resonant OKE measurement of an aqueous solution, it is not immediately evident whether a slow picosecond component originates from the reorientation of the solute or from solvent water whose dynamics have been modified by the presence of the solute (Figure 1).

Although the OKE response of neat water is known to be weak and to decay within the sub-picosecond regime[8], it has not been established whether a slower

ACCEPTED MANUSCRIPT

picosecond component observed in aqueous solutions can be assigned to solute reorientation. For example, previous OKE studies of aqueous solutions have often assigned slow picosecond components to hydration-water or hydrogen-bond-network dynamics, reflecting the fact that non-resonant OKE detects the collective polarizability response of all components in solution [14]. At the same time, in concentrated solutions of optically anisotropic solutes, a solute-associated contribution can also become significant because the orientational OKE response depends strongly on molecular polarizability anisotropy. Therefore, whether a slow picosecond component mainly reflects hydration-water dynamics, solute-associated reorientational relaxation, or a coupled solute–solvent response must be evaluated for each system.

In this work, heterodyne-detected OKE spectroscopy is employed to investigate the reorientational dynamics of three amino acids (alanine, proline, and lysine monohydrochloride) in aqueous solution and to examine whether non-resonant OKE can resolve solute reorientation. Systematic measurements as functions of concentration, temperature, and chirality, together with control experiments using aqueous poly(vinyl alcohol) (PVA) solutions[3,6], support the assignment of the slow picosecond response to amino acid reorientation. These measurements establish the origin of the slow OKE response and provide insight into the local environment governing the rotational motion of amino acids in aqueous solution.

Experimental methods

Solubility measurements of amino acids

All the chemical compounds were purchased from either Merck, TCI, or Wako and used as received. The purities were as follows: L-alanine (>99.0 %), D-alanine (>98.0 %), L-valine (>98.0 %), D-valine (single spot by TLC), L-arginine (>99.0 %), D-arginine

ACCEPTED MANUSCRIPT

(single spot by TLC), L-phenylalanine (>98.0 %), D-phenylalanine (>98.0 %), L-proline (>98.0 %), D-proline (>98.0 %), L-lysine monohydrochloride (>98.0 %), and D-lysine monohydrochloride (>98.0 %). Solubility was determined from UV–Vis absorbance measurements using calibration curves constructed according to the Lambert–Beer law. Absorbance measurements were performed using a UV–Vis spectrometer. Calibration curves were obtained by linear regression of absorbance versus concentration at the following wavelengths: alanine (207 nm), valine (207 nm), arginine (221 nm), phenylalanine (257 nm), proline (213 nm), and lysine monohydrochloride (217 nm). The concentrations used for calibration were 10, 20, and 50 mM for alanine, arginine, phenylalanine, proline, and lysine monohydrochloride, and 3, 6, and 15 mM for valine. Saturated aqueous solutions were prepared by adding an excess amount of each amino acid to water at room temperature and stirring for several hours to reach equilibrium. After equilibration, the suspensions were centrifuged at 10000 g for 5 min to remove undissolved solids, and the supernatants were collected. The pH values of the supernatants were as follows: alanine (6.08), arginine (11.4), phenylalanine (5.73), lysine hydrochloride (5.48), proline (7.03), and valine (6.34). The supernatants were diluted 10-fold prior to measurement, except for racemic lysine monohydrochloride, which was measured without dilution. The solubilities were calculated using the corresponding calibration curve, taking into account the dilution factor.

Optical Kerr effect spectroscopy

Ultrafast OKE spectroscopy measurements were performed using a regenerative amplified Ti:sapphire laser system (Spectra-Physics Mai Tai and Solstice), delivering pulses with a duration of approximately 70 fs at a repetition rate of 1 kHz and a central wavelength of 800 nm. The output beam was split into pump and probe pulses. The

ACCEPTED MANUSCRIPT

pump pulses were generated by directing a portion of the fundamental output into an optical parametric amplifier (Light Conversion, TOPAS), producing tunable pulses centered at 694 nm. The pump beam polarization was adjusted to 45° with respect to the probe polarization using a polarizer. The pump beam was weakly focused onto the sample with a lens, yielding a typical beam diameter of approximately 300 μm at the sample position. The crossing angle between the pump and probe beams at the sample was kept below 10° to ensure effective spatial overlap. The probe beam was derived directly from the 800 nm fundamental output. It was focused onto the sample to a beam diameter of approximately 120 μm. Before the sample, a motorized polarizer (P1) and a precisely controlled quarter-wave plate (QWP) were installed. The transmission axis of P1 and the fast axis of the QWP were initially aligned at 0°. Heterodyne detection was implemented by rotating P1 by ±2° relative to this position and taking the differential signal between the two measurements[1,3,4,10]. This procedure enables sensitive detection of pump-induced birefringence with linear sensitivity to the third-order nonlinear polarization. Details of the heterodyne detection scheme and calibration procedures are described in our previous publication[4].

After transmission through the sample, the probe beam passed through an analyzer (P2) oriented at 90° with respect to the initial probe polarization. This crossed-polarizer configuration selectively detects changes in the probe polarization induced by transient birefringence in the sample. A color filter was placed in front of the detector to suppress scattered pump light and eliminate pump-induced artifacts. The transmitted probe intensity was recorded as a function of the pump–probe delay to obtain time-resolved OKE signals.

Temperature-dependent measurements were performed by attaching a thermistor-controlled resistive heater (Thorlabs) to the sample cell to regulate the

ACCEPTED MANUSCRIPT

sample temperature. The cell was wrapped in aluminum foil to improve thermal conduction and ensure a uniform temperature across the cell. Spectra were recorded at 25, 45, 65, and 85 °C, with the sample allowed to equilibrate at each temperature before measurement.

Curve fitting

The reorientational relaxation time τ was obtained by fitting the linear region of each OKE decay to a single exponential,

$$I(t) = A\exp\left(-\frac{t - t_0}{\tau}\right) \qquad (eq.1)$$

where I is the OKE signal intensity, A is the amplitude at t_0, t is the delay time, t_0 is the start of the fitting range, and τ is the time constant of the signal decay, taken as the reorientational relaxation time. Because the signal intensity and laser-induced artifacts varied among the datasets, the fitting range was selected separately for each experimental series. The endpoint of each fitting range was defined as the time at which the signal had decayed to approximately ~10^{-2} (a.u.), and had effectively reached the noise floor. The starting point was selected after the fast sub-picosecond response and any laser-induced artifacts had decayed

Because the signal intensity and the laser-derived artifacts differed between datasets, the fitting range was chosen individual experimental sets. The fitting terminal range is the signal decayed to ~10^{-2} (a.u.), at which point it has essentially reached the noise floor. The start of the fitting range was set after the fast sub-picosecond response and any laser-derived artifacts, and was chosen separately for each series. For pure water and the PVA solutions, whose decays are themselves sub-picosecond, the fit was started at 0.7 ps. For the temperature-dependent measurements (Figure 4), it was started at 8 ps, because the faster decays at higher temperatures would otherwise leave too few data

ACCEPTED MANUSCRIPT

points if a later start were used. For the concentration-dependent measurements (Figure 5), it was started at 20 ps to exclude a laser-derived noise feature appearing near 20 ps. Regardless of the fitting range selected, each sample yielded consistent decay times, as demonstrated in Figures 4 and 5.

Results and Discussions

Selection of model amino acids

Optical Kerr effect (OKE) spectroscopy is a third-order nonlinear technique, and the measured signal contains contributions from both solute and solvent. Sensitivity to the reorientational dynamics of the solute therefore requires relatively concentrated solutions, typically on the order of 1 M or higher. We therefore surveyed the aqueous solubilities of a series of amino acids and selected those with the highest solubility (Table S1).

Figure S2 and Table S1 summarize the solubilities of enantiopure (L and D) and racemic forms of representative amino acids in aqueous solution. The solubilities of alanine, valine, and phenylalanine determined here are in good agreement with the classical values reported[15]. The calibration curves obtained from UV–vis spectroscopy are shown in Figure S1. For simple aliphatic amino acids such as alanine and valine (Figure S2 a,b), the solubilities of the L-, D-, and racemic forms are nearly identical within experimental uncertainty.

In contrast, amino acids bearing additional functional groups exhibit more pronounced differences between racemic and enantiopure systems. For arginine, the racemic form shows a slightly higher solubility than the enantiopure forms (Figure S2c), whereas the racemic form is clearly less soluble than the enantiopure forms for phenylalanine and lysine monohydrochloride (Figure S2d,f).

ACCEPTED MANUSCRIPT

Among the six amino acids, alanine, proline, and lysine monohydrochloride exhibited the highest aqueous solubilities, all dissolving well above 1 M, whereas valine, phenylalanine, and arginine were appreciably less soluble. The former three were therefore selected as model systems: they combine high aqueous solubility with good optical transparency, and span a range of side-chain sizes, allowing the reorientational dynamics to be compared across solutes of different molecular volume. Lysine monohydrochloride, which additionally exhibits a chirality-dependent solubility, further serves as a system in which to examine whether chirality influences the reorientational dynamics. We confirmed the resulting precipitation of racemic-lysine monohydrochloride is racemic crystals (Figure S3). The single crystal analysis of obtained D-,L- and racemic crystals are shown in Supporting Information.

Origin of the picosecond reorientational component in Optical Kerr effect spectroscopy

OKE spectroscopy probes the time-dependent anisotropic polarizability of a medium induced by an intense pump pulse. The measured signal consists of two principal contributions: an ultrafast electronic response occurring on sub-picosecond timescales (typically < 1 ps), and a slower nuclear response originating from molecular motions. The latter includes both low-frequency intermolecular vibrational modes and diffusive reorientational relaxation of molecules in solution. While the electronic component reflects the instantaneous electronic polarization, the nuclear component provides direct insight into molecular dynamics and intermolecular interactions in the liquid phase.

Although several groups have reported OKE signals from amino acid derived solutions, most studies have primarily focused on low-frequency vibrational responses in the terahertz or depolarized Raman frequency range[5,16]. In contrast, the reorientational relaxation dynamics of amino acids in solution have received far less

ACCEPTED MANUSCRIPT

attention. In the present work, we focus exclusively on the diffusive reorientational relaxation component, which directly reflects rotational Brownian motion and its coupling to the local hydrodynamic environment.

To verify that the OKE setup is sensitive to solute dynamics under the present experimental conditions, we first measured the OKE signal of pure water (Figure 3a). The water signal exhibited a fast relaxation component with a time constant of approximately 0.7 ps, consistent with previously reported ultrafast orientational relaxation of bulk water[8]. This result also confirms that the instrumental response and data analysis procedures are appropriate for resolving sub-picosecond dynamics.

We then measured aqueous solutions of L-alanine, L-proline, and L-lysine monohydrochloride. In contrast to pure water, each amino acid solution exhibited a clear, slower picosecond component in addition to the fast water response (Figure 3a). Because the reorientational relaxation of pure water occurs on a sub-picosecond timescale, the slower component observed in the amino acid solutions initially seems to be attributed to solute reorientation. However, the addition of the solute also increases the solution viscosity and may thereby slow the dynamics of water. It is therefore not immediately clear whether the slow component originates from solute reorientation or from viscosity-slowed water dynamics.

To examine these two possibilities, we used aqueous poly(vinyl alcohol) (PVA; 0.2, 0.5, 1.0, and 2.0 wt%) solutions as control samples. The macroscopic viscosity increased monotonically with PVA concentration, reaching approximately eightfold greater than that for pure water (Figure 3b). Since the reorientational relaxation of a polymer of this size (Mw: 85,000−124,000) is expected to be far slower than our picosecond observation window, no resolvable reorientational component of the

ACCEPTED MANUSCRIPT

polymer itself should be observed. The OKE response of the PVA solutions is therefore expected to be dominated by the dynamics of water.

The reorientational relaxation time τ of each decay was obtained by (eq.1). According to the Stokes–Einstein–Debye (SED) relation, this reorientation time is proportional to the hydrodynamic volume of the rotating species and to the friction it experiences,

$$\tau = \frac{V\eta}{k_{\mathrm{B}}T} \qquad (eq.2)$$

where V, η, k_{B}, and T are the effective hydrodynamic molecular volume, the solution viscosity, the Boltzmann constant, and the absolute temperature, respectively[1]. If the slow component in Figure 3c arose from water slowed by the increased viscosity, a comparable slow component should also appear in the PVA solutions, particularly at higher PVA concentrations, where the macroscopic viscosity was even greater. However, τ remained almost unchanged from the value of pure water even as the viscosity increased (Figure 3d, Table S2). Instead, the OKE reponses of all PVA solutions remained within 2.5 ps, remaining very close to that of pure water despite the increase in viscosity (Figure 3c, Table S2). No additional slow picosecond component appeared with increasing PVA concentration.

The slower picosecond component in Figure 3a can therefore be assigned primarily to amino acid associated reorientational dynamics rather than to viscosity-slowed bulk water. Accordingly, the extracted relaxation time provides a probe of the local rotational friction associated with the amino acids.

Reorientation dynamics of amino acids in aqueous solution

The three amino acids were first compared at 1 M and 25 °C. Although their macroscopic viscosities are nearly equal (Figure S4), the time constants for

ACCEPTED MANUSCRIPT

reorientational relaxation (τ) are 11, 12, and 26 ps for alanine, proline, and lysine monohydrochloride, respectively (Figure 4a–c). In particular, lysine monohydrochloride exhibited a relaxation time approximately twice those of alanine and proline. The difference in τ reflects the molecular size as expected from Eq. (2).

For all three amino acids, the decay became faster with increasing temperature (Figure 4a–c). According to the SED relation (Eq. (2)), the reorientation time (τ) should be linearly related to η/T. The viscosities of the amino-acid solutions were measured using a rheometer and were found to be comparable to that of water at room temperature. Because rheology measurements at high temperature were difficult due to the evaporation and concomitant precipitation, the viscosities at those temperatures were estimated using the correlation reported by Kestin *et al* [17]. When τ was plotted against η/T (Figure 4d), proline and alanine showed a nearly linear relationship, whereas lysine monohydrochloride deviated slightly from linearity. This deviation in lysine monohydrochloride solutions may suggest that the local solvation environment of lysine monohydrochloride differs from those of alanine and proline.

According to Eq. (2), the slope of a plot of τ against η/T is proportional to the effective hydrodynamic molecular volume. The obtained slopes for alanine, proline, and lysine monohydrochloride solutions were 3384.7 ± 281, 3277.9 ± 106 and 5711.3 ± 1010 ps・K・mPa^{-1}・s^{-1}, respectively. Alanine and proline have comparable molecular sizes, whereas lysine monohydrochloride is substantially larger. To provide a quantitative consistency, we estimated the van der Waals molecular volumes (V_{vdw}) from the optimized DFT geometries using standard atomic van der Waals radii (see the DFT calculation section in the Supporting Information). The obtained volumes were 83.4, 107.0, and 145.5 Å^3 for alanine, proline, and lysine, respectively. Although these geometric volumes should not be compared directly with the SED-derived effective

ACCEPTED MANUSCRIPT

hydrodynamic volumes (V_{eff}), the relative increase from alanine to lysine is consistent with the larger effective volume obtained from the SED analysis. Furthermore, we estimated the orientational OKE contribution from the molecular polarizability anisotropy. DFT calculations at 700 nm gave much larger polarizability anisotropies for the amino acids than for water (Table S3). Because the orientational OKE contribution is expected to scale approximately with $c\gamma^2$, where c is the molar concentration and γ is the polarizability anisotropy, the amino-acid contribution is estimated to exceed that of water even at 0.25 M[18]. This comparison does not exclude hydration-water or solute–water network contributions, but supports the presence of a substantial amino-acid-associated contribution to the slow picosecond OKE response.

Furthermore, to characterize the temperature dependence of the OKE relaxation from an activation-energy perspective, we performed an Arrhenius-type analysis according to eq. 3,

$$\tau = \tau_0 \exp\left(\frac{E_a}{RT}\right) \qquad (eq.3)$$

where E_a and R are the apparent activation energy for the observed OKE relaxation and the gas constant, respectively. The results are summarized in Figure S5. The Arrhenius plots were linear for all three amino-acid solutions over the measured temperature range, yielding apparent activation energies of 14.0, 12.4, and 9.5 kJ mol^{-1} for alanine, proline, and lysine monohydrochloride, respectively. The comparable magnitudes of these values indicate that the temperature dependence of the slow OKE relaxation is governed by a similar thermally activated process in the three systems. Notably, lysine monohydrochloride exhibited the longest relaxation time but the smallest apparent activation energy, suggesting that its slower relaxation reflects its larger effective hydrodynamic volume and local rotational friction rather than from a larger activation barrier.

ACCEPTED MANUSCRIPT

We next investigated the concentration dependency using L-lysine monohydrochloride solutions. Figure 5a shows the OKE signals of L-lysine monohydrochloride solutions at several concentrations (0.25, 0.50, 1.0, and 2.8 M). As established above, the slow picosecond component reflects the reorientation of lysine monohydrochloride itself rather than that of the surrounding water. The reorientation time τ increased monotonically with concentration (Figure 5b, Table S5). Within the SED framework, the monotonic increase of τ reflects a growing rotational friction around the solute as the solution becomes more concentrated. The concentration dependence of the viscosity of electrolyte and amino acid solutions is commonly described by the Jones–Dole equation[19–21],

$$\frac{\eta}{\eta_0} = 1 + \mathrm{A}\sqrt{c} + \mathrm{B}c \qquad (eq.4)$$

where η_0 is the viscosity of the pure solvent and c the solute concentration. The $\mathrm{A}\sqrt{c}$ term arises from long-range electrostatic interactions between solutes, whereas the $\mathrm{B}c$ term reflects short-range solute–solvent and solute–solute contacts. Since OKE reports the local friction around the solute, it is the short-range $\mathrm{B}c$ contribution that is most relevant here; the near-linear increase of τ with concentration is consistent with this crowding-dominated, short-range friction.

Additionally, the amplitude A of the slow exponential component (eq.1) extracted from unnormalized OKE traces also increased approximately with lysine monohydrochloride concentration (Table S6). This trend supports a concentration-dependent amino-acid-associated contribution to the slow OKE response, although the amplitude is not used for quantitative decomposition of solute and solvent contributions.

We also examined whether enantiomeric composition affects the concentration-dependent local rotational friction of lysine monohydrochloride. Because the increase in τ with concentration reflects enhanced solute–solute and solute–solvent contacts,

ACCEPTED MANUSCRIPT

racemic and enantiopure solutions could show different relaxation times if homochiral and heterochiral contacts contributed differently to the local friction. However, no measurable difference was observed among D-, L-, and racemic lysine monohydrochloride within experimental uncertainty over the entire concentration range (Figure S6 and Table S5).

Discussion

The present results indicate that the reorientation time τ obtained from OKE reflects not the macroscopic viscosity of the solution but the local rotational friction in the vicinity of the solute. In the PVA control experiment, increasing the macroscopic viscosity left τ unchanged from the value of pure water. This viscosity increase is therefore likely dominated by polymer-chain-mediated stress relaxation on mesoscopic to macroscopic length scales, while the local rotational environment of water remains nearly unchanged on the sub-picosecond timescale.

In the amino acid solutions, by contrast, τ differed markedly among the solutes even when their macroscopic viscosities were nearly equal, and it increased monotonically with concentration, indicating a concentration-dependent change in the friction experienced at the molecular scale. These observations demonstrate that OKE provides access to local rotational friction, or molecular-scale microviscosity, arising from the solvation environment surrounding the solute and is therefore complementary to conventional rheometry.

The approximately linear concentration dependence of τ is also qualitatively consistent with the Jones–Dole equation, which is associated with short-range solute–solvent and solute–solute interactions, providing additional support for this interpretation.

The present interpretation does not exclude hydration-water or solute–water hydrogen-bond-network dynamics[14]. However, our results are more consistent with the

ACCEPTED MANUSCRIPT

interpretation that the slow component reflects a substantial amino-acid-associated contribution. This assignment is supported by several observations. First, increasing the macroscopic viscosity with PVA did not generate a comparable slow OKE component. Second, the SED-derived V_{eff} shows the same qualitative size trend as the DFT-estimated V_{vdw}, despite a systematic offset of approximately a factor of two between the static geometric and effective hydrodynamic volumes. Third, DFT calculations show that the polarizability anisotropies of the amino acids are much larger than that of water. Because the heterodyne-detected orientational OKE amplitude is expected to scale approximately with $c\gamma^2$, the amino-acid contribution is estimated to exceed that of water even at 0.25 M. Together with the concentration-dependent increase in the slow-component amplitude, these results support assigning the slow response to amino-acid-associated reorientational relaxation rather than to bulk-water relaxation alone under the present conditions.

We also examined whether enantiomeric composition affects the local rotational friction of lysine monohydrochloride. No measurable difference was observed among D-, L-, and racemic solutions, indicating that any contribution of stereochemically specific contacts to the ensemble-averaged rotational friction is below the sensitivity of the present OKE measurements.

Conclusion

In this study, we used ultrafast OKE spectroscopy to investigate the reorientational dynamics of three amino acids (alanine, proline, and lysine monohydrochloride) in aqueous solutions, examined in terms of concentration, temperature, and chirality. Using PVA as a control, we showed that the OKE reorientation time τ is unchanged even when the macroscopic viscosity is increased, demonstrating that the picosecond component originates from the rotation of the solute itself. The results indicate that

ACCEPTED MANUSCRIPT

OKE provides information on the local rotational friction associated with the solute and is therefore complementary to rheometry, which measures the macroscopic viscosity of the solution. τ increased in the order of molecular size and rose monotonically with concentration, consistent with the SED law and short-range term of the Jones–Dole equation. These results provide new kinetic insight into the orientational dynamics of amino acids in aqueous solution.

Funding details

・Japan Science and Technology Agency (JST) CREST: JPMJCR20T4

・Japan Science and Technology Agency (JST) ACT-X: JPMJAX23D8

・Japan Society for the Promotion of Science (JSPS) KAKENHI (JP24H00470, JP24H01693, JP24K17742, JP26K01484, JP26H013257)

・Murata Science and Education Foundation (M25AN123)

・ Hirose Foundation

・Toyo Gousei Foundation.

Author Contributions

S. K. conceived the concept of this work. S. K. and T. N. designed the experimental approach. K. M., T. N. T.S. and S. K. carried out the experiments. S. K. and K. M. drafted and reviewed manuscript. Supervisory tasks were handled by S. K., T. N., K. S., and Y. Y. All authors discussed, commented, and have given approval to the final version of the manuscript.

ACCEPTED MANUSCRIPT

Disclosure statement

No potential conflict of interest was reported by the author(s).

Acknowledgement

This work was financially supported by CREST (JPMJCR20T4) and ACT-X (JPMJAX23D8) from Japan Science and Technology Agency (JST), KAKENHI (JP24H00470, JP24H01693, JP20J00845, JP24K17742, JP26K01484, JP26H013257 (Transformative Research Area A, "π-complexity")) from Japan Society for the Promotion of Science (JSPS), DAAD (91612715), Murata Science and Education Foundation(M25AN123), Hirose Foundation, and Toyo Gousei Foundation. Supports from University of Tsukuba, KUINS and Kumano Dormitory community, Kyoto University, for providing a stimulating academic environment are also gratefully acknowledged.

Reference

[1] Zhong Q, Fourkas JT. Optical Kerr Effect Spectroscopy of Simple Liquids. J Phys Chem B. 2008;112(49):15529–15539.

[2] Righini R. Ultrafast Optical Kerr Effect in Liquids and Solids. Science. 1993;262(5138):1386–1390.

[3] Hunt NT, Jaye AA, Meech SR. Ultrafast dynamics in complex fluids observed through the ultrafast optically-heterodyne-detected optical-Kerr-effect (OHD-OKE). Phys Chem Chem Phys. 2007;9(18):2167.

[4] Kushida S, Wang K, Genet C, et al. Ultrafast Dynamics of Solute Molecules Probed by Resonant Optical Kerr Effect Spectroscopy. J Phys Chem Lett. 2022;13(40):9309–9315.

[5] Mazur K, Heisler IA, Meech SR. Ultrafast Dynamics and Hydrogen-Bond Structure in Aqueous Solutions of Model Peptides. J Phys Chem B. 2010;114(32):10684–10691.

[6] Palombo F, Heisler IA, Hribar-Lee B, et al. Tuning the Hydrophobic Interaction: Ultrafast Optical Kerr Effect Study of Aqueous Ionene Solutions. J Phys Chem B. 2015;119(29):8900–8908.

ACCEPTED MANUSCRIPT

[7] Idrissi A, Bartolini P, Ricci M, et al. Temperature dependence of the reorientational dynamics and low-frequency response of aqueous urea solutions investigated by femtosecond optical Kerr-effect spectroscopy and molecular-dynamics simulation. Phys Chem Chem Phys. 2003;5(20):4666.

[8] Palese S, Schilling L, Miller RJD, et al. Femtosecond optical Kerr effect studies of water. J Phys Chem. 1994;98(25):6308–6316.

[9] Shah Y, Meech SR, Heisler IA. Ultrafast Optical Kerr Effect Spectroscopy Reveals the Vibrational Fingerprint of Acetate–Water Hydrogen Bonds. ACS Omega. 2025;59840−59848.

[10] Kushida S, Wang K, Seidel M, et al. Fluidic Molecular Dynamics and Energy Relaxation Pathways in Solution-State Electronic Strong Coupling Using a High-Mode-Number Cavity. J Phys Chem Lett. 2025;16(33):8570–8579.

[11] Turton DA, Wynne K. Universal nonexponential relaxation: Complex dynamics in simple liquids. J Chem Phys. 2009;131(20):201101.

[12] Winkler K, Lindner J, Bürsing H, et al. Ultrafast Raman-induced Kerr-effect of water: Single molecule versus collective motions. J Chem Phys. 2000;113(11):4674–4682.

[13] Torre R, Bartolini P, Righini R. Structural relaxation in supercooled water by time-resolved spectroscopy. Nature. 2004;428:296–299.

[14] Mazur K, Heisler IA, Meech SR. THz Spectra and Dynamics of Aqueous Solutions Studied by the Ultrafast Optical Kerr Effect. J Phys Chem B. 2011;115(11):2563–2573.

[15] Dalton JB, Schmidt Carl LA. The solubilities of certain amino acids in water, the densities of their solutions at twenty-five degrees, and the calculated heats of solution and partial molal volumes. J Biol Chem. 1933;103(2):549–578.

[16] Giraud G, Wynne K. Time-Resolved Optical Kerr-Effect Spectroscopy of Low-Frequency Dynamics in Di- L -alanine, Poly- L -alanine, and Lysozyme in Solution. J Am Chem Soc. 2002;124(41):12110–12111.

[17] Kestin J, Sokolov M, Wakeham WA. Viscosity of liquid water in the range −8 °C to 150 °C. J Phys Chem Ref Data. 1978;7(3):941–948.

[18] Lin CH, Heritage JP, Gustafson TK, et al. Birefringence arising from the reorientation of the polarizability anisotropy of molecules in collisionless gases. Phys Rev A. 1976;13(2):813–829.

[19] Jones G, Dole M. THE VISCOSITY OF AQUEOUS SOLUTIONS OF STRONG ELECTROLYTES WITH SPECIAL REFERENCE TO BARIUM CHLORIDE. J Am Chem Soc. 1929;51(10):2950–2964.

[20] Jenkins HDB, Marcus Y. Viscosity B-Coefficients of Ions in Solution. Chem Rev. 1995;95(8):2695–2724.

ACCEPTED MANUSCRIPT

[21] Wynne K. The Mayonnaise Effect. J Phys Chem Lett. 2017;8(24):6189–6192.

Figures

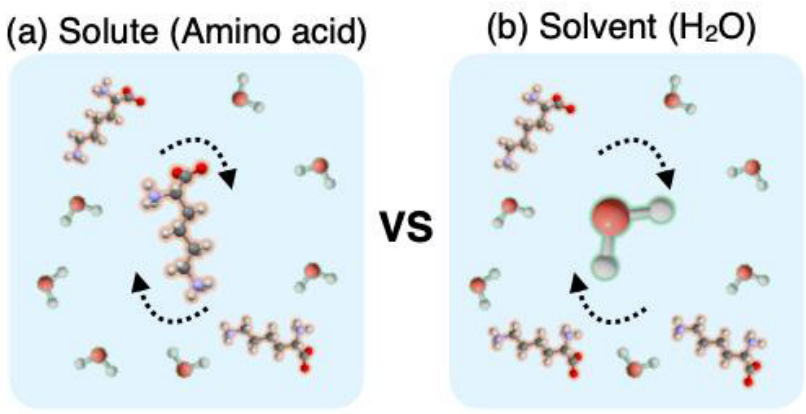


Figure 1 Two possible origins of the picosecond component in the OKE signal of an aqueous amino acid solution: reorientation of (a) the solute (amino acid) itself, or (b) the solvent water (slowed by the increased viscosity).

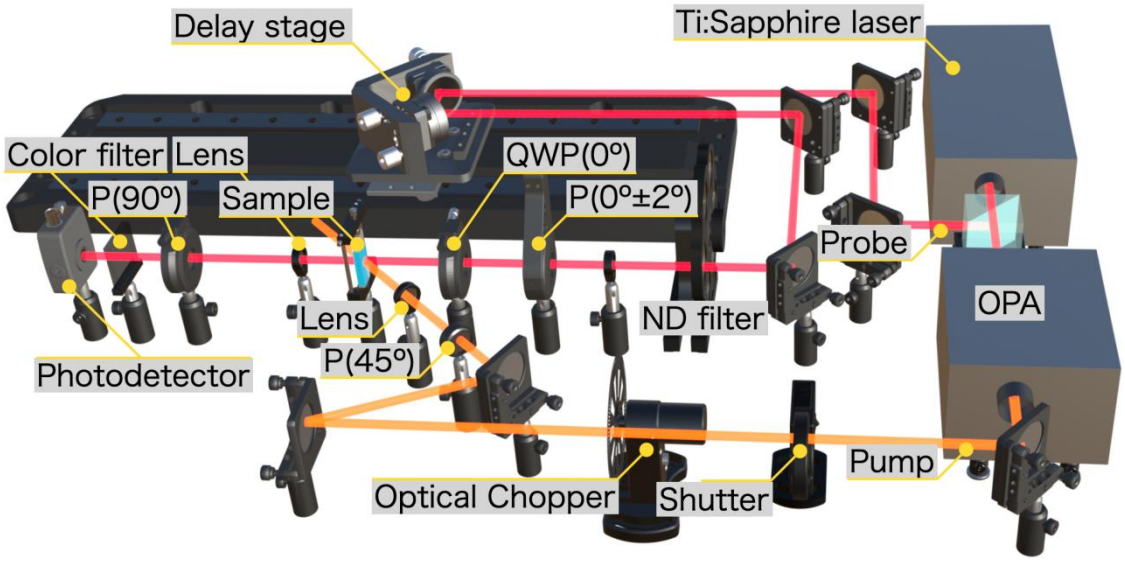


Figure 2. An illustration of experimental setup for OKE spectroscopy. P and QWP refer to polarizer and quarter waveplate, respectively.

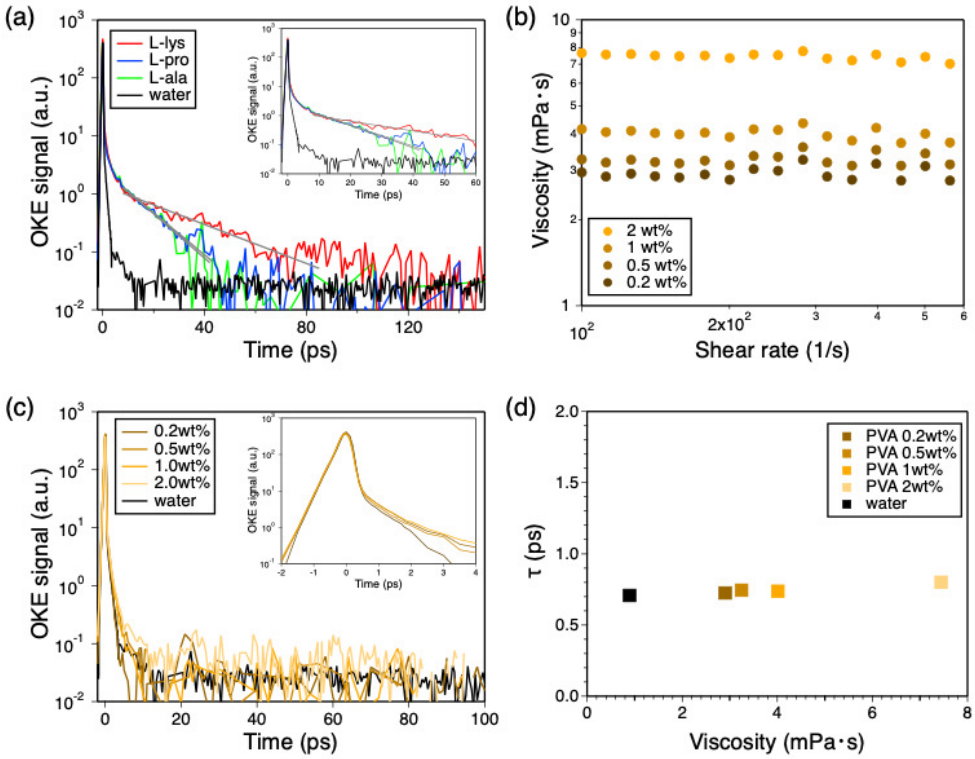


Figure 3. (a) OKE signals of 1 M aqueous L-alanine (green), L-proline (blue), L-lysine monohydrochloride (red), and pure water (black) at 25 °C; the inset shows an expanded view over the first 60 ps. (b) Viscosity of aqueous PVA solutions (0.2, 0.5, 1.0, and 2.0 wt%) measured with a rheometer as a function of shear rate. (c) OKE signals of the same PVA solutions and pure water (black); the inset shows the response near time zero. (d) τ plotted against macroscopic viscosity for the PVA solutions, and water. The viscosity of water is taken from the literature values[17].

ACCEPTED MANUSCRIPT

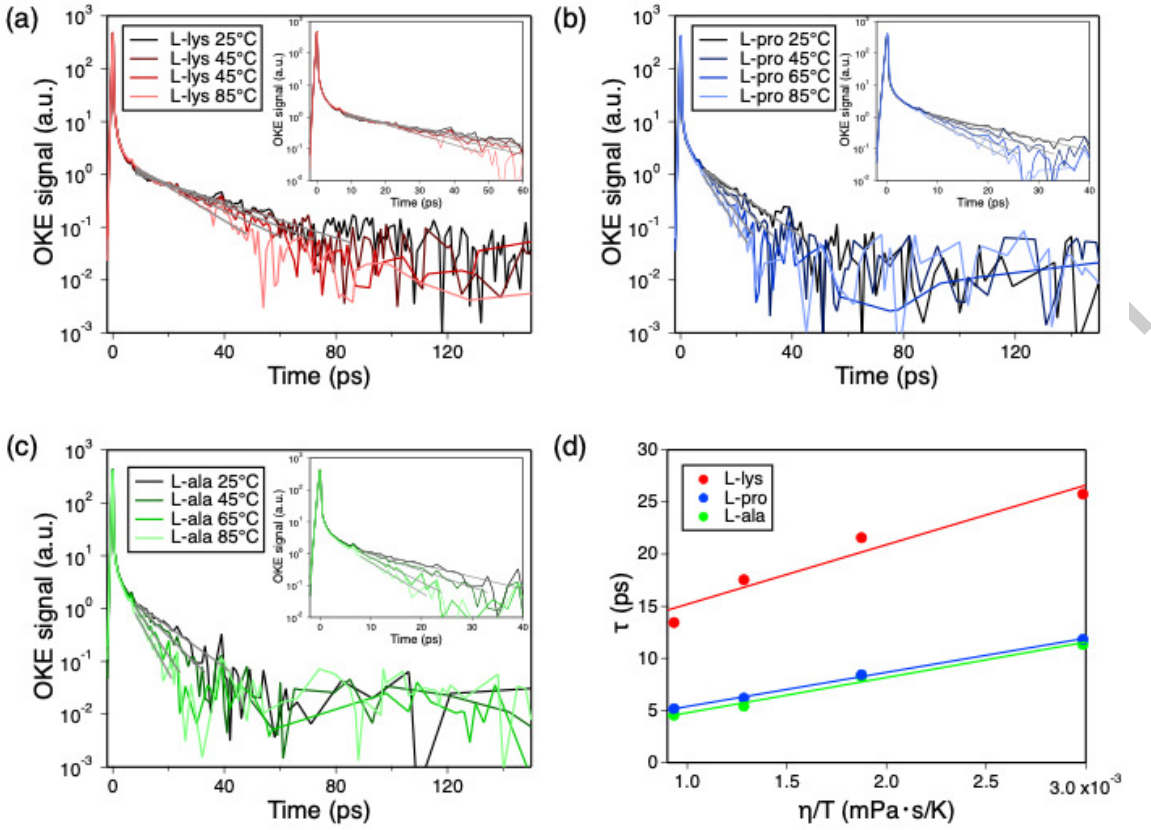


Figure 4. (a–c) OKE signals of 1 M aqueous (a) L-lysine monohydrochloride, (b) L-proline, and (c) L-alanine at 25, 45, 65, and 85 °C; the insets show expanded views at early times. (d) τ plotted against η/T, where η is the viscosity of water taken from the literature[17], for L-lysine monohydrochloride (red), L-proline (blue), and L-alanine (green).

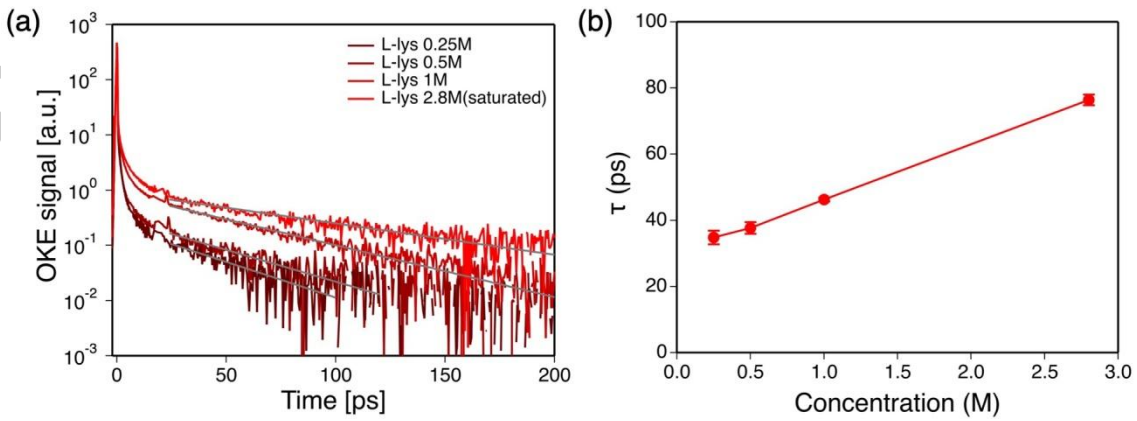
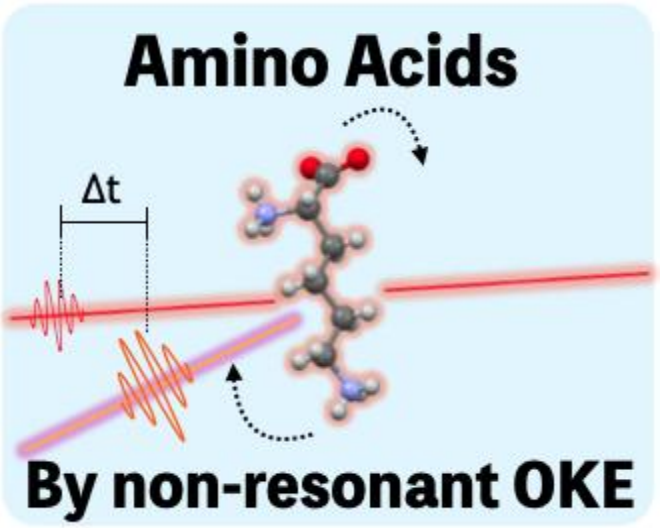


Figure 5. OKE signals at different concentrations for (a) L-lysine monohydrochloride solutions. The concentrations are 0.25, 0.50, 1.0, and 2.8 M, indicated from dark to light colors. (b) τ as a function of concentration.

ACCEPTED MANUSCRIPT



スクリーンショット 2026-07-06 11.37.12

ACCEPTED MANUSCRIPT

Supporting Information

Reorientational Dynamics of Amino Acids in Aqueous Solution Probed by Ultrafast Optical Kerr Effect Spectroscopy

Koichi Murakami[a], Tomohiro Nobeyama[a,b], Yuta Koda[a], Takahiro Sasamori[a], Kentaro Shiraki[a], Yohei Yamamoto[a,c], and Soh Kushida[a]**

*corresponding author:

Dr. Soh Kushida, Institute of Pure and Applied Sciences, University of Tsukuba, Tsukuba 305-8573, Japan

Prof. Yohei Yamamoto, Institute of Pure and Applied Sciences, Tsukuba Research Center for Energy Materials Science (TREMS) and Hydrogen Boride Research Center, Tsukuba Institute for Advanced Research, University of Tsukuba, Tsukuba 305-8573, Japan

Email: s-kushida@ims.tsukuba.ac.jp, yamamoto@ims.tsukuba.ac.jp

ACCEPTED MANUSCRIPT

Table of Contents

1. General Information ---------- S2
2. Experimental Section ---------- S2
3. Supporting Figures and Tables ---------- S4
4. Single Crystal Analysis ---------- S10
5. Calculations for collision frequency ---------- S13
6. DFT Calculation ---------- S14
7. Supporting Reference ---------- S18

1. General Information

Unless otherwise noted, all chemical compounds and solvents were used as received from either Merck Co., Ltd., WAKENYAKU CO.,LTD. or Tokyo Chemical Industry Co., Ltd. Optical components—including polarizers, wave plates, mirrors, beam splitters, filters, lenses, and others—were purchased from Thorlabs, Inc. Sigma Koki or Newport Corporation. UV–vis absorption spectra were recorded using a commercial spectrophotometer (JASCO V-570). OKE (Optical Kerr Effect) measurements were performed with a home-built apparatus. The delay stage and lock-in amplifier were controlled via Python scripts. Data processing and curve fitting were conducted using Python.

2. Experimental Section

Sample Preparation

Solutions: Each amino acid solution was prepared by dissolving the corresponding amino acid in distilled water. The initial amounts of amino acid and water were adjusted to yield a slightly higher concentration than the target value, as dissolution of the amino acid results in a change in the total solution volume and consequently affects the final concentration. The mixture was stirred until complete dissolution. The solution was then adjusted to the final volume using a graduated cylinder to obtain the desired concentration.

Viscosity measurement

The viscosities of the aqueous PVA solutions (0.2, 0.5, 1.0, and 2.0 wt%) and of the 1 M amino-acid solutions (L-alanine, L-proline, and L-lysine monohydrochloride) were measured with a rotational rheometer (Anton Paar, MCR 301) at 25 °C. Flow curves

ACCEPTED MANUSCRIPT

were recorded as a function of shear rate, and the viscosity of each solution was taken from the Newtonian region.

Single Crystal Analysis:

Single crystals of racemi_a, D, and L were obtained after recrystallization from water solution at room temperature. Intensity data of racemi_a, D, and L were collected on a Bruker APEX-II system using Mo-Ka radiation (λ = 0.71073 Å). The structures were solved using SHELXT-2018[S1] and refined by a full-matrix least-squares method on F^2 for all reflections using SHELXL-2018.[1] All non-hydrogen atoms were refined anisotropically, and the all hydrogen atoms were refined isotropically. Crystallographic data for racemi_a: $C_6H_{15}ClN_2O_2$, FW 182.65, crystal size 0.25×0.15×0.10 mm^3, temperature –170 ˚C, monoclinic, space group $P2_1/a$ (#14), a = 8.5308(1) Å, b = 11.1431(1) Å, c = 9.1365(1) Å, β = 105.8894(14)˚, V = 835.327(16) Å^3, Z = 4, D_{calcd} = 1.452 g cm^{-3}, μ = 0.412 mm^{-1}, θ_{max} = 33.629˚, 33741 reflections measured, 3206 independent reflections (R_{int} = 0.0148), 160 parameters refined, GOF = 1.115, completeness = 99.3%, R_1 [$I > 2\sigma(I)$] = 0.0201, wR_2 (all data) = 0.0560, largest diff. peak and hole 0.510 and –0.227 e Å^{-3}. D: $C_6H_{19}ClN_2O_4$, FW 218.68, crystal size 0.20×0.15×0.12 mm^3, temperature –170 ˚C, monoclinic, space group $P2_1$ (#4), a = 5.8646(1) Å, b = 13.2180(2) Å, c = 7.4120(1) Å, β = 97.9459(12)˚, V = 569.049(15) Å^3, Z = 2, D_{calcd} = 1.276 g cm^{-3}, μ = 0.326 mm^{-1}, θ_{max} = 33.609˚, 15909 reflections measured, 4084 independent reflections (R_{int} = 0.0106), 194 parameters refined, GOF = 1.089, completeness = 99.5%, R_1 [$I > 2\sigma(I)$] = 0.0166, wR_2 (all data) = 0.0448, largest diff. peak and hole 0.275 and –0.190 e Å^{-3}. L: $C_6H_{19}ClN_2O_4$, FW 218.68, crystal size 0.20×0.18×0.05 mm^3, temperature –170 ˚C, monoclinic, space group $P2_1$ (#4), a = 5.8691(1) Å, b = 13.2195(3) Å, c = 7.4146(2) Å, β = 98.010(2)˚, V = 569.66(2) Å^3, Z =

ACCEPTED MANUSCRIPT

2, D_{calcd} = 1.275 g cm^{-3}, μ = 0.326 mm^{-1}, θ_{max} = 33.540°, 19051 reflections measured, 4034 independent reflections (R_{int} = 0.0122), 194 parameters refined, GOF = 1.133, completeness = 100.0%, R_1 [$I > 2\sigma(I)$] = 0.0176, wR_2 (all data) = 0.0475, largest diff. peak and hole 0.233 and –0.267 e Å^{-3}.

ACCEPTED MANUSCRIPT

3. Supporting Figures and Tables

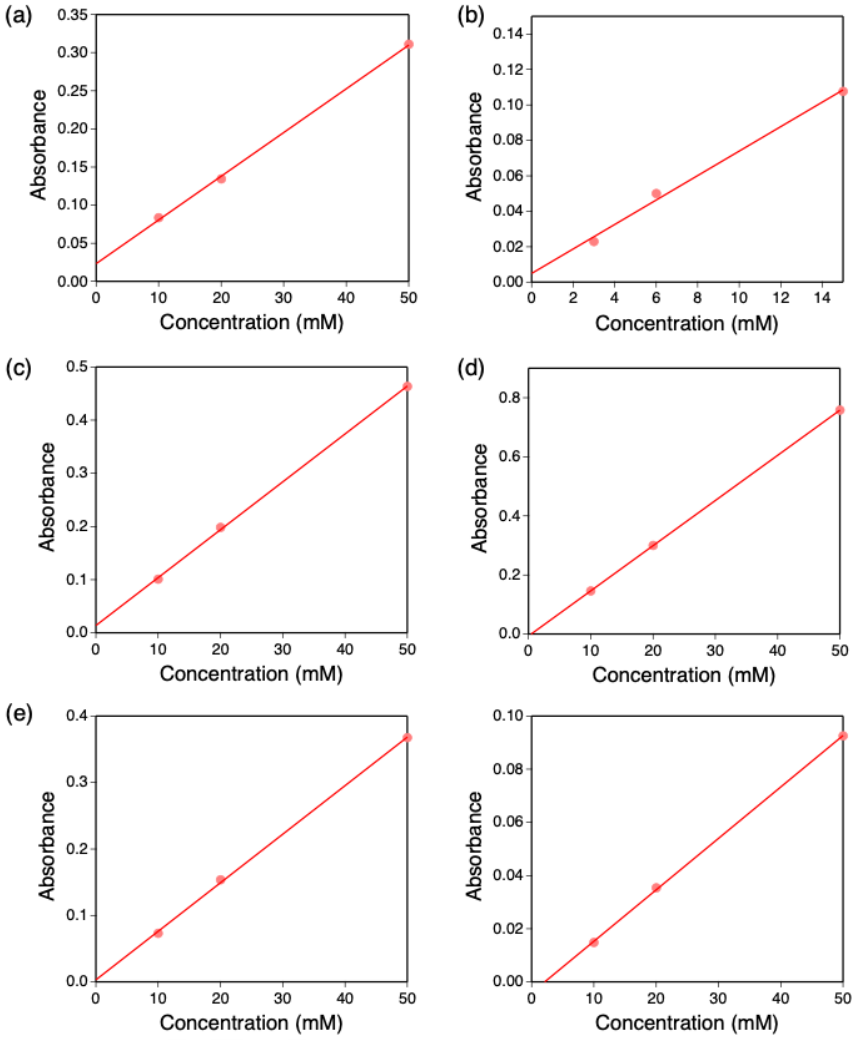


Figure S1. Calibration curves of (a) alanine (207 nm), (b) valine (207 nm), (c) arginine (221 nm), (d) phenylalanine (257 nm), (e) proline (213 nm), and (f) lysine (217 nm) obtained by UV–Vis spectroscopy. The data were fitted using least-squares linear regression.

ACCEPTED MANUSCRIPT

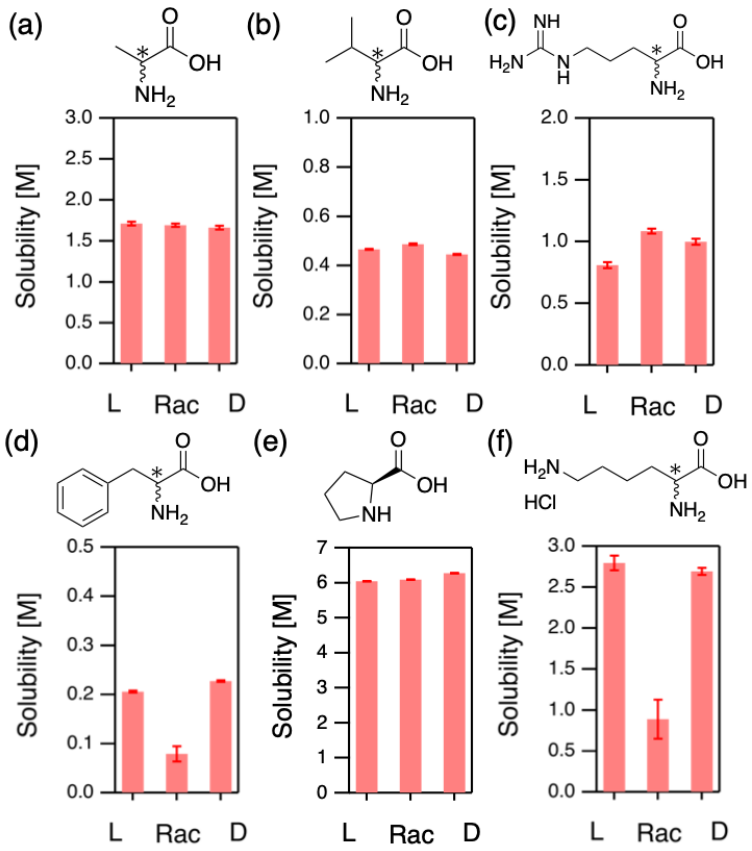


Figure S2. Solubilities of enantiopure (L and D) and racemic amino acids in aqueous solution. The amino acids are (a) alanine, (b) valine, (c) arginine, (d) phenylalanine, and (e) proline, (f) lysine monohydrochloride. The molecular structures of each amino acid are shown above the corresponding plots. Error bars represent standard deviations obtained from repeated measurements.

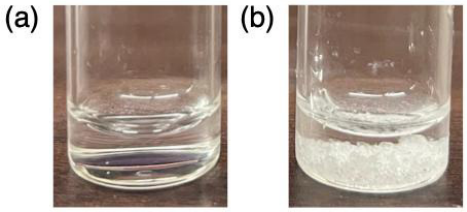


Figure S3. Photographs of aqueous lysine monohydrochloride solutions prepared at an initial concentration of 2.8 M: (a) enantiopure (L-) and (b) racemic.

ACCEPTED MANUSCRIPT

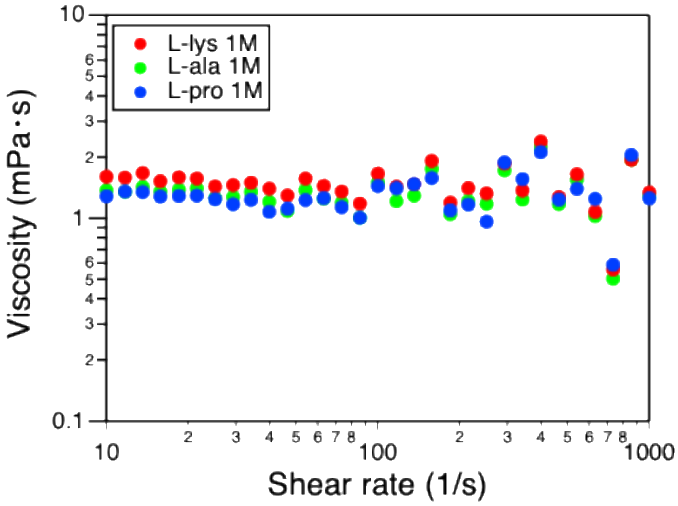


Figure S4. Viscosity of 1 M aqueous L-alanine (green), L-proline (blue), and L-lysine monohydrochloride (red) at 25 °C, measured by rheometer as a function of shear rate. The three solutions have nearly identical viscosities.

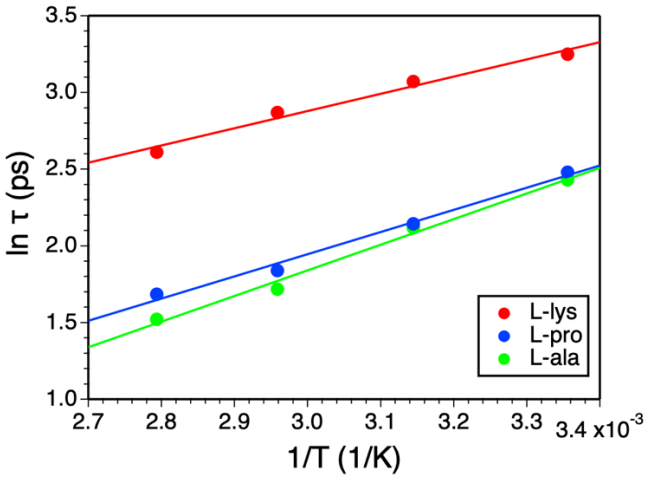


Figure S5. Arrhenius plots of the reorientation time for L-lysine monohydrochloride (red), L-proline (blue), and L-alanine (green); the solid lines are linear fits, yielding apparent activation energies of 14.0, 12.4, and 9.5 kJ mol-1 for alanine, proline, and lysine monohydrochloride, respectively.

ACCEPTED MANUSCRIPT

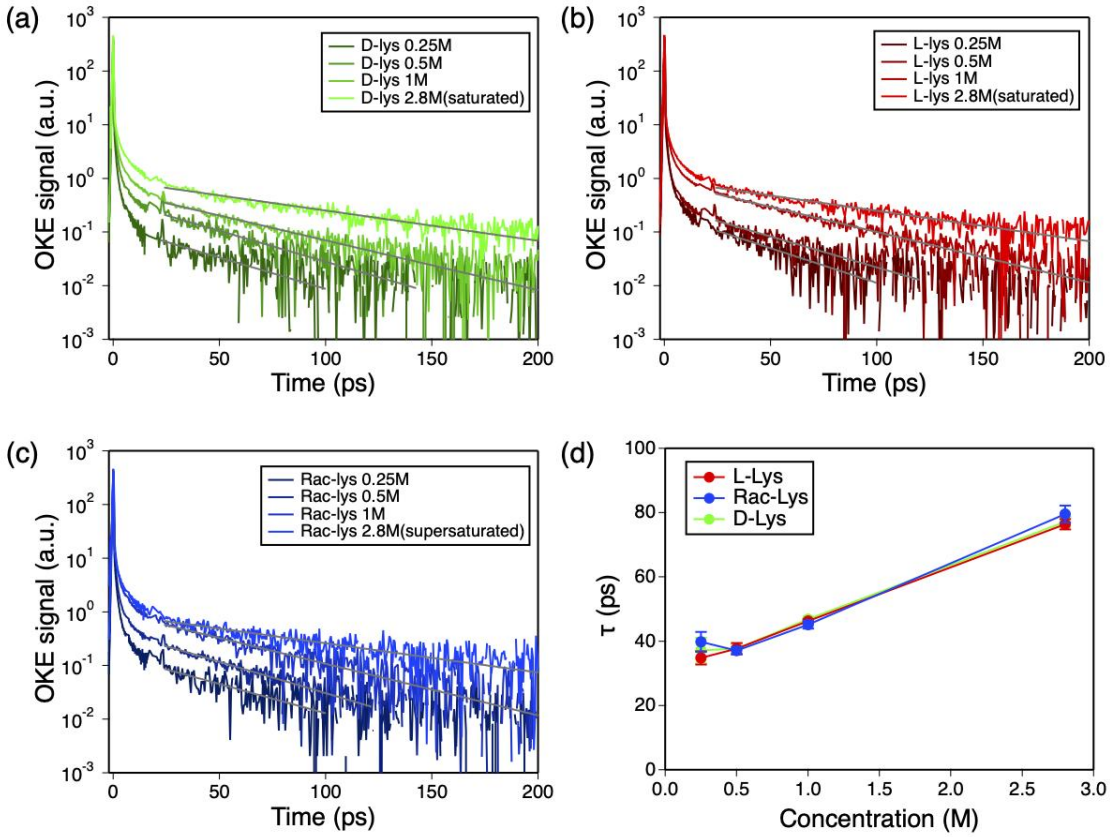


Figure S6. OKE signals at different concentrations for (a) D-, (b) L-, and (c) Rac-lysine monohydrochloride solutions. The concentrations are 0.25, 0.50, 1.0, and 2.8 M, indicated from dark to light colors. (d) τ as a function of concentration.

Table S1. Solubilities of enantiopure (L and D) and racemic amino acids in aqueous solution.

Amino acids	S_L (M)	S_D (M)	S_{Rac} (M)
Alanine	1.691 ± 0.009	1.640 ± 0.009	1.680 ± 0.009
Valine	0.560 ± 0.009	0.553 ± 0.009	0.567 ± 0.009
Arginine	0.907 ± 0.007	1.062 ± 0.016	1.085 ± 0.020
Phenylalanine	0.163 ± 0.0005	0.164 ± 0.0005	0.0772 ± 0.0004
Proline	6.046 ± 0.010	6.278 ± 0.001	6.089 ± 0.010

ACCEPTED MA

Lysine・HCl	2.756 ± 0.005	2.759 ± 0.005	1.198 ± 0.001

ACCEPTED MANUSCRIPT

Table S2. Reorientational relaxation time of pure water and aqueous PVA solutions.

Sample	τ (ps)
Water	0.7 ± 0.01
PVA 2wt%	0.8 ± 0.01
PVA 1wt%	0.7 ± 0.01
PVA 0.5wt%	0.7 ± 0.01
PVA 0.2wt%	0.7 ± 0.01

Table S3. DFT-derived polarizability parameters at 700 nm. The polarizability anisotropy γ was obtained from the frequency-dependent polarizability tensor $\alpha(-\omega;\omega)$ at 700 nm.

Sample	γ / au	γ^2 / au²
L-lysine	23.63	558.52
L-alanine	18.8	353.45
L-proline	20.35	414
water	0.335	0.112

Table S4. Reorientational relaxation time of 1 M aqueous L-alanine, L-proline, and L-lysine monohydrochloride at 25, 45, 65, and 85 °C.

Sample	25 ℃ (ps)	45 ℃ (ps)	65 ℃ (ps)	85 ℃ (ps)
L-lysine	25.8 ± 0.8	21.6 ± 0.6	17.5 ± 0.4	13.5 ± 0.4
L-alanine	11.3 ± 0.5	8.2 ± 0.3	5.4 ± 0.2	4.6 ± 0.3
L-proline	11.8 ± 0.4	8.4 ± 0.4	6.2 ± 0.2	5.2 ± 0.2

ACCEPTED MANUSCRIPT

Table S5. Reorientational relaxation time of lysine monohydrochloride aqueous solutions with different enantiomeric ratios and concentrations.

Sample	0.25 M (ps)	0.5 M (ps)	1 M (ps)	2.8 M (ps)
L-lysine	33.6 ± 2.0	37.7 ± 1.8	46.3 ± 0.6	76.4 ± 1.6
D-lysine	37.2 ± 3.9	37.7 ± 1.5	46.9 ± 0.8	77.1 ± 1.5
Rac-Lysine	39.8 ± 3.1	37.1 ± 1.1	45.2 ± 1.2	79.6 ± 2.65

ACCEPTED MANUSCRIPT

Table S6. Slow-component amplitudes A obtained from single-exponential fits to the unnormalized OKE traces of D-, L-, and racemic lysine monohydrochloride solutions at different concentrations.

Sample	0.25 M (a.u.)	0.5M (a.u.)	1M (a.u.)	2.8M (a.u.)
L-lysine	0.150 ± 0.008	0.198 ± 0.006	0.591 ± 0.007	0.730 ± 0.011
D-lysine	0.066 ± 0.004	0.259 ± 0.008	0.402 ± 0.006	0.727 ± 0.011
Rac-Lysine	0.108 ± 0.005	0.271 ± 0.005	0.645 ± 0.012	0.714 ± 0.016

Table S7. Effective hydrodynamic volumes derived from the SED analysis and DFT-estimated van der Waals volumes of alanine, proline, and lysine monohydrochloride.

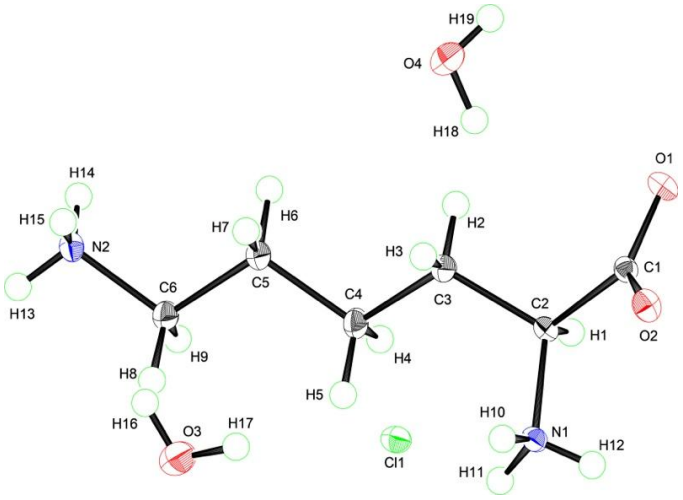
Sample	Slope S ($ps \cdot K \cdot mPa^{-1} \cdot s^{-1}$)	V_{eff} ($Å^3$)[a]	V_{vdw} ($Å^3$)[b]
L-alanine	3384.7 ± 281	46.7 ± 3.9	83.4
L-proline	3277.9 ± 106	45.3 ± 1.5	107
L-lysine monohydrochloride	5711.3 ± 1010	78.9 ± 13.9	145.5

a: Estimated from OKE experiments. b: Estimated from DFT calculations.

ACCEPTED MANUSCRIPT

4. Single Crystal Analysis

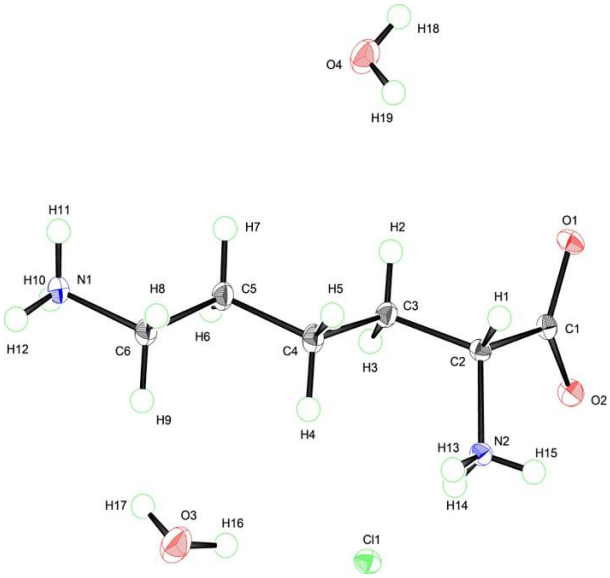
Table S8. Crystal structure, crystal data and structure refinement for L-lysine.



Identification code	L	
Empirical formula	C6 H19 Cl N2 O4	
Formula weight	218.68	
Temperature	103(2) K	
Wavelength	0.71073 Å	
Crystal system	Monoclinic	
Space group	$P2_1$ **(#4)**	
Unit cell dimensions	a = 5.86910(10) Å	a= 90°.
	b = 13.2195(3) Å	b= 98.010(2)°.
	c = 7.4146(2) Å	g = 90°.
Volume	569.66(2) $Å^3$	
Z	2	
Density (calculated)	1.275 Mg/m^3	
Absorption coefficient	0.326 mm^{-1}	
F(000)	236	
Crystal size	0.200 x 0.180 x 0.050 mm^3	
Theta range for data collection	2.774 to 33.540°.	
Index ranges	-9<=h<=9, -20<=k<=20, -11<=l<=11	
Reflections collected	19051	
Independent reflections	4034 [R(int) = 0.0122]	
Completeness to theta = 25.242°	100.0 %	
Refinement method	Full-matrix least-squares on F^2	
Data / restraints / parameters	4034 / 1 / 194	
Goodness-of-fit on F^2	1.133	
Final R indices [I>2sigma(I)]	R1 = 0.0176, wR2 = 0.0473	
R indices (all data)	R1 = 0.0180, wR2 = 0.0475	
Absolute structure parameter	0.004(8)	
Extinction coefficient	n/a	
Largest diff. peak and hole	0.233 and -0.267 $e.Å^{-3}$	

ACCEPTED MANUSCRIPT

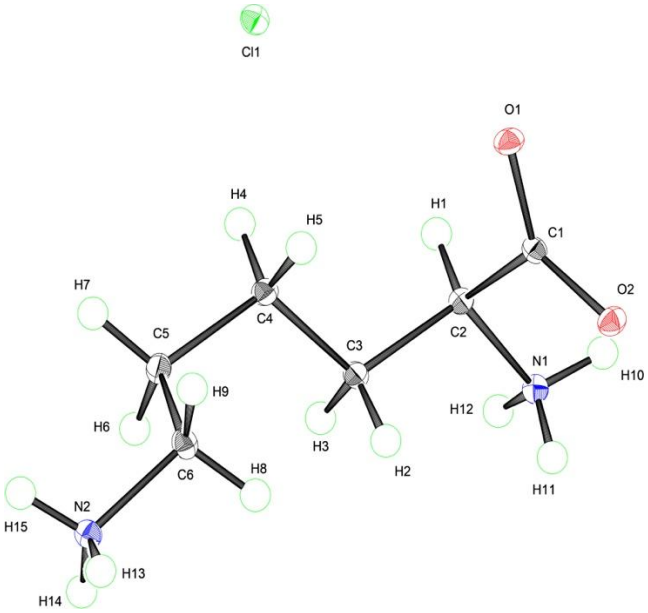
Table S9. Crystal structure, crystal data and structure refinement for D-lysine.



Identification code	D	
Empirical formula	C6 H19 Cl N2 O4	
Formula weight	218.68	
Temperature	103(2) K	
Wavelength	0.71073 Å	
Crystal system	Monoclinic	
Space group	$P2_1$ **(#4)**	
Unit cell dimensions	a = 5.86460(10) Å	a= 90°.
	b = 13.2180(2) Å	b= 97.9459(12)°.
	c = 7.41200(10) Å	g = 90°.
Volume	569.049(15) $Å^3$	
Z	2	
Density (calculated)	1.276 Mg/m^3	
Absorption coefficient	0.326 mm^{-1}	
F(000)	236	
Crystal size	0.200 x 0.150 x 0.120 mm^3	
Theta range for data collection	2.775 to 33.609°.	
Index ranges	-9<=h<=9, -20<=k<=19, -11<=l<=10	
Reflections collected	15909	
Independent reflections	4084 [R(int) = 0.0106]	
Completeness to theta = 25.242°	99.5 %	
Refinement method	Full-matrix least-squares on F^2	
Data / restraints / parameters	4084 / 1 / 194	
Goodness-of-fit on F^2	1.089	
Final R indices [I>2sigma(I)]	R1 = 0.0166, wR2 = 0.0448	
R indices (all data)	R1 = 0.0167, wR2 = 0.0448	
Absolute structure parameter	0.008(8)	
Extinction coefficient	n/a	
Largest diff. peak and hole	0.275 and -0.190 $e.Å^{-3}$	

ACCEPTED MANUSCRIPT

Table S10. Crystal structure, crystal data and structure refinement for Rac-lysine



Identification code	racemi_a	
Empirical formula	C6 H15 Cl N2 O2	
Formula weight	182.65	
Temperature	103(2) K	
Wavelength	0.71073 Å	
Crystal system	monoclinic	
Space group	$P2_1/a$ (#14)	
Unit cell dimensions	a = 8.53080(10) Å	a= 90°.
	b = 11.14310(10) Å	b= 105.8894(14)°.
	c = 9.13650(10) Å	g = 90°.
Volume	835.327(16) $Å^3$	
Z	4	
Density (calculated)	1.452 Mg/m^3	
Absorption coefficient	0.412 mm^{-1}	
F(000)	392	
Crystal size	0.250 x 0.150 x 0.100 mm^3	
Theta range for data collection	2.952 to 33.629°.	
Index ranges	-13<=h<=13, -17<=k<=17, -14<=l<=14	
Reflections collected	33741	
Independent reflections	3206 [R(int) = 0.0148]	
Completeness to theta = 25.242°	99.3 %	
Refinement method	Full-matrix least-squares on F^2	
Data / restraints / parameters	3206 / 0 / 160	
Goodness-of-fit on F^2	1.115	
Final R indices [I>2sigma(I)]	R1 = 0.0201, wR2 = 0.0557	
R indices (all data)	R1 = 0.0205, wR2 = 0.0560	
Extinction coefficient	n/a	
Largest diff. peak and hole	0.510 and -0.227 $e.Å^{-3}$	

ACCEPTED MANUSCRIPT

5. Calculations for collision frequency

To estimate the frequency of intermolecular encounters in concentrated lysine solutions, we employed a diffusion-controlled collision model based on the Stokes–Einstein relation. The translational diffusion coefficient D was approximated using

$$D = \frac{k_B T}{6\pi\eta r_h}$$

where k_B is the Boltzmann constant, T is the absolute temperature (298 K), η is the solution viscosity, and r_h is the hydrodynamic radius of lysine.

For the 2.8 M lysine solution, we assumed $\eta = 10$ mPa·s and $r_h = 0.5$nm,[2] yielding $D \approx 4.4 \times 10^{-11}$m² s⁻¹. The diffusion-controlled collision rate constant for identical molecules was estimated using the Smoluchowski expression:

$$k_{diff} = 8\pi DR$$

where R is the encounter distance, approximated as $R = 2r_h$. Under these assumptions, $k_{diff} \approx 1.1 \times 10^{-18}$m³ s⁻¹. The collision frequency per molecule at concentration (C) was then estimated as

$$f \approx k_{diff}\, n$$

where $n = 1000\, N_A C$ is the number density with N_A denoting Avogadro's constant (6.022×10^{23} mol⁻¹). For $C = 2.8$ mol L⁻¹, this yields $f \sim 2 \times 10^9$ s⁻¹, corresponding to an average intermolecular encounter every ~ 0.5 ns. This estimated collision timescale is many orders of magnitude shorter than the characteristic timescale of crystallization (typically ~hours), indicating that nucleation cannot be limited by simple diffusive

ACCEPTED MANUSCRIPT

encounters but instead requires rare, orientation-specific configurations.

ACCEPTED MANUSCRIPT

6. DFT calculation

All ab initio and density functional theory (DFT) calculations were performed by using Gaussian 16 Rev.A.03 or Rev.B.01 and results were visualized with Gaussview6[3, 4]. All geometries were optimized using density functional theory (DFT) at the B3LYP/aug-cc-pvtz level of theory without any symmetry assumptions. Harmonic vibration frequency analysis was performed at the same level of theory to verify all stationary points as local minima (with no imaginary frequency). The size of molecule was calculated from the optimized coordination by getting diameter value as the longest distance between the center of gravity and atoms for each molecule. As for the polarity, we conducted a single point calculation with the following keywords: Polar, pop=full, CPHF=Rdfreq, int=grid=ultrafine.

L-alanine

Optimized Cartesian coordinates (Å)

N	1.23818300	-1.15346700	0.12910900
C	0.58092100	0.17916900	0.40804000
C	1.25996300	1.30480000	-0.35384100
C	-0.92409800	-0.01041100	0.03744900
O	-1.22438300	-1.15702700	-0.39783500
O	-1.66377700	0.97019700	0.21551900
H	0.42124700	-1.72200000	-0.20543900
H	1.94823900	-1.10479900	-0.59791500
H	1.65555300	-1.57775600	0.95292000
H	0.64763200	0.35078700	1.47948300
H	0.74057000	2.23627400	-0.14418500

ACCEPTED MANUSCRIPT

H	2.30056900	1.41523900	-0.04986900
H	1.22347600	1.12980800	-1.43011500

Frequency-dependent polarizability tensor at 700 nm

Alpha(-ω;ω), ω = 700 nm

Dipole polarizability tensor in the Gaussian molecular coordinate system.

	(au)	(10**-24 esu)	(10**-40 SI)
iso	0.636504D+02	0.943202D+01	0.104945D+02
aniso	0.188002D+02	0.278591D+01	0.309974D+01
xx	0.514999D+02	0.763149D+01	0.849118D+01
yx	0.134635D+01	0.199509D+00	0.221984D+00
yy	0.688172D+02	0.101977D+02	0.113464D+02
zx	0.147947D+01	0.219234D+00	0.243931D+00
zy	-0.150418D+01	-0.222896D+00	-0.248006D+00
zz	0.706342D+02	0.104669D+02	0.116460D+02

L-proline

Optimized Cartesian coordinates (Å)

N	0.70763700	-1.02510600	0.57897900
C	1.98636600	-0.60838300	-0.10497600
C	1.61771400	0.70293800	-0.78753900
C	0.65546200	1.36087400	0.20940100
C	-0.18091400	0.19405500	0.75172300
C	-1.48557400	-0.09143900	-0.05161400
O	-2.35288600	0.79737100	-0.01719800
O	-1.51760300	-1.20237800	-0.64833000
H	0.88318500	-1.51508600	1.45118700

ACCEPTED MANUSCRIPT

H	0.10628300	-1.62382100	-0.02917000
H	2.73738700	-0.46091000	0.66643800
H	2.30674100	-1.40165300	-0.77305700
H	1.11908900	0.50969900	-1.73774300
H	2.49938900	1.30744900	-0.98609900
H	0.01801400	2.11519400	-0.24327400
H	1.21415900	1.83021400	1.01916100
H	-0.43211800	0.30643900	1.80195900

Frequency-dependent polarizability tensor at 700 nm

Alpha(-ω;ω), ω = 700 nm

Dipole polarizability tensor in the Gaussian molecular coordinate system.

	(au)	(10**-24 esu)	(10**-40 SI)
iso	0.843808D+02	0.125039D+02	0.139125D+02
aniso	0.203471D+02	0.301513D+01	0.335478D+01
xx	0.739220D+02	0.109541D+02	0.121881D+02
yx	-0.258368D+01	-0.382862D+00	-0.425991D+00
yy	0.857067D+02	0.127004D+02	0.141311D+02
zx	0.542775D+01	0.804310D+00	0.894916D+00
zy	-0.214191D+01	-0.317398D+00	-0.353153D+00
zz	0.935138D+02	0.138573D+02	0.154183D+02

L-lysine

Optimized Cartesian coordinates (Å)

N	1.72186400	1.78677300	-0.03799100

ACCEPTED MANUSCRIPT

C	1.50327100	0.49090900	0.71126900
C	0.02819800	0.10090000	0.78179100
C	-0.62934600	-0.20728700	-0.56804400
C	-2.08322100	-0.68140700	-0.45408000
C	-3.07246600	0.39868300	-0.02529000
N	-4.44337600	-0.13493300	0.00161300
C	2.41846200	-0.56075400	0.00675100
O	3.08215900	-0.11931600	-0.97214500
O	2.41015100	-1.70586300	0.48552300
H	2.08829200	2.53149100	0.54841700
H	2.43180300	1.49818600	-0.75444800
H	0.88459100	2.13089800	-0.50168500
H	1.88550900	0.64236400	1.71776000
H	-0.02256700	-0.78520700	1.41480900
H	-0.51360500	0.88914100	1.30770400
H	-0.04972500	-0.98353700	-1.07142600
H	-0.60130100	0.66822200	-1.22542100
H	-2.40482000	-1.07244300	-1.42180000
H	-2.13453200	-1.51785000	0.25077000
H	-3.04818400	1.21626400	-0.74966800
H	-2.77252900	0.82154800	0.94044200
H	-5.09669300	0.59711100	0.25509000
H	-4.52352100	-0.84390700	0.72270100

Frequency-dependent polarizability tensor at 700 nm

Alpha(-ω;ω), ω = 700 nm

ACCEPTED MANUSCRIPT

Dipole polarizability tensor in the Gaussian molecular coordinate system.

	(au)	(10**-24 esu)	(10**-40 SI)
iso	0.116349D+03	0.172411D+02	0.191833D+02
aniso	0.236330D+02	0.350205D+01	0.389656D+01
xx	0.120859D+03	0.179095D+02	0.199270D+02
yx	0.104114D+02	0.154281D+01	0.171660D+01
yy	0.111433D+03	0.165127D+02	0.183729D+02
zx	-0.744537D+01	-0.110329D+01	-0.122758D+01
zy	0.836782D-01	0.123998D-01	0.137967D-01
zz	0.116753D+03	0.173011D+02	0.192500D+02

Water

Optimized Cartesian coordinates (Å)

H	0.00000000	-0.77781100	1.52378900
O	0.00000000	-0.02950700	0.91724400
H	0.00000000	0.74613100	1.48881800

Frequency-dependent polarizability tensor at 700 nm

Alpha(-ω;ω), ω = 700 nm

Dipole polarizability tensor in the Gaussian molecular coordinate system.

	(au)	(10**-24 esu)	(10**-40 SI)
iso	0.105481D+02	0.156306D+01	0.173914D+01
aniso	0.335288D+00	0.496845D-01	0.552815D-01
xx	0.104277D+02	0.154523D+01	0.171930D+01
yx	0.000000D+00	0.000000D+00	0.000000D+00
yy	0.107714D+02	0.159615D+01	0.177596D+01

ACCEPTED MANUSCRIPT

zx	0.000000D+00	0.000000D+00	0.000000D+00
zy	0.129327D-02	0.191642D-03	0.213231D-03
zz	0.104451D+02	0.154781D+01	0.172217D+01

The polarizability anisotropy was calculated from the frequency-dependent polarizability tensor at 700 nm as

$$\gamma^2 = \frac{1}{2}[(\alpha_{xx} - \alpha_{yy})^2 + ((\alpha_{yy} - \alpha_{zz})^2 + (\alpha_{zz} - \alpha_{xx})^2] + 3(\alpha_{xy}{}^2 + \alpha_{xz}{}^2 + \alpha_{yz}{}^2)$$

The orientational OKE contribution was then estimated using the approximate scaling $A_{OKE} \propto c\gamma^2$, where c is the molar concentration.

ACCEPTED MANUSCRIPT

7. References

[1] Usón I, Sheldrick GM. An introduction to experimental phasing of macromolecules illustrated by *SHELX*; new autotracing features. Acta Crystallogr D Struct Biol. 2018;74(2):106–116.

[2] Patil, KC, Gowardipe A. Volumetric, ultrasonic and viscometric studies on L-lysine mono-hydrochloride in aqueous medium at different temperatures. IJRAT. 2019;7(4):453–458.

[3] M. J. Frisch, G. W. T., H. B. Schlegel, G. E. Scuseria, ; M. A. Robb, J. R. C., G. Scalmani, V. Barone, ; G. A. Petersson, H. N., X. Li, M. Caricato, A. V. Marenich, ; J. Bloino, B. G. J., R. Gomperts, B. Mennucci, H. P. Hratchian, ; J. V. Ortiz, A. F. I., J. L. Sonnenberg, D. Williams-Young, ; F. Ding, F. L., F. Egidi, J. Goings, B. Peng, A. Petrone, ; T. Henderson, D. R., V. G. Zakrzewski, J. Gao, N. Rega, ; G. Zheng, W. L., M. Hada, M. Ehara, K. Toyota, R. Fukuda, ; J. Hasegawa, M. I., T. Nakajima, Y. Honda, O. Kitao, H. Nakai, ; T. Vreven, K. T., J. A. Montgomery, Jr., J. E. Peralta, ; et al. conputer code GAUSSIAN 16 revision A.03, Gaussian, Inc 2016.

[4] M. J. Frisch, G. W. T., H. B. Schlegel, G. E. Scuseria, ; M. A. Robb, J. R. C., G. Scalmani, V. Barone, ; G. A. Petersson, H. N., X. Li, M. Caricato, A. V. Marenich, ; J. Bloino, B. G. J., R. Gomperts, B. Mennucci, H. P. Hratchian, ; J. V. Ortiz, A. F. I., J. L. Sonnenberg, D. Williams-Young, ; F. Ding, F. L., F. Egidi, J. Goings, B. Peng, A. Petrone, ; T. Henderson, D. R., V. G. Zakrzewski, J. Gao, N. Rega, ; G. Zheng, W. L., M. Hada, M. Ehara, K. Toyota, R. Fukuda, ; J. Hasegawa, M. I., T. Nakajima, Y. Honda, O. Kitao, H. Nakai, ; T. Vreven, K. T., J. A. Montgomery, Jr., J. E. Peralta, ; et al. conputer code GAUSSIAN 16 revision B.01, Gaussian, Inc 2016

ACCEPTED MANUSCRIPT

Non-resonant OKE, together with the viscosity controls, reveals amino acid associated reorientational dynamics and local rotational friction in aqueous solution beyond macroscopic viscosity.

ACCEPTED MANUSCRIPT